ACS APPLIED MATERIALS & INTERFACES

Research Article

www.acsami.org

Structure Engineering of Hole–Conductor Free Perovskite-Based Solar Cells with Low-Temperature-Processed Commercial Carbon Paste As Cathode

Fuguo Zhang,[†] Xichuan Yang,*[,†] Haoxin Wang,[†] Ming Cheng,[†] Jianghua Zhao,[†] and Licheng Sun[†,‡]

[†]Institute of Artificial Photosynthesis, State Key Laboratory of Fine Chemicals, DUT–KTH Joint Education and Research Centre on Molecular Devices, Dalian University of Technology (DUT), 2 Linggong Road, 116024 Dalian, China

[‡]School of Chemical Science and Engineering, Center of Molecular Devices, Department of Chemistry, Royal Institute of Technology (KTH), Teknikringen 30, 10044 Stockholm, Sweden

Supporting Information

ABSTRACT: Low-temperature-processed (100 °C) carbon paste was developed as counter electrode material in hole–conductor free perovskite/TiO_2 heterojunction solar cells to substitute noble metallic materials. Under optimized conditions, an impressive PCE value of 8.31% has been achieved with this carbon counter electrode fabricated by doctor-blading technique. Electrochemical impedance spectroscopy demonstrates good charge transport characteristics of low-temperature-processed carbon counter electrode. Moreover, this carbon counter electrode-based perovskite solar cell exhibits good stability over 800 h.

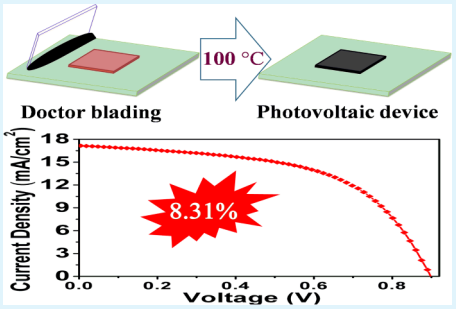

KEYWORDS: *low temperature, commercial carbon paste, hole–conductor free, perovskite, heterojunction solar cell*

1. INTRODUCTION

Great attention has been drawn to developing cost-effective, high-efficiency solar cells to meet the ever increasing demand for clean energy. The emerging solid-state thin film solar cells are considered to be a promising technology to fulfill this target.[1−4] Although solid-state junction devices assembled with silicon and compound semiconductors show high efficiency and dominate the commercial market, the indispensable need for expensive materials and complex manufacturing processes restrict their large-scale production.

Recently, methylammonium lead halide ($CH_3NH_3PbX_3$, X = Cl, Br, I) and its mixed halide crystals, corresponding to three-dimensional perovskite structures,[5,6] have invoked tremendous amount of scientific and commercial interests for their notable characteristics of easily tunable properties, direct band gap, large absorption coefficient, high carrier mobility, simple solution approaches, and their potential in fabricating cost-effective solid-state thin film solar cells.[7−9] To date, for Perovskite-based solar cells, extraordinary power conversion efficiencies (PCE) ranging from 12 to more than 19% have been obtained through optimization of preparing technology and device structure,[10−21] which make it competitive in future commercialization. However, noble metals such as Au or Ag acting as counter electrodes (CEs) are indispensable in these high-performance photovoltaic devices, and are not conducive for large-scale production. Besides, the high-energy-consumption vacuum evaporation method of preparing costly metal cathodes restrains its commercialization as well. Therefore, replacement of precious metal cathode is urgently required for this high-efficiency photovoltaic device.

Carbon is a good choice for its abundance, low cost, and appropriate energy level. Different types carbon materials, such as carbon nanotube, carbon fiber, graphene, and so on, have been applied in many other photovoltaic devices successfully and impressive results have been achieved.[22−25] For most reported carbon materials, high-temperature treatments are necessary, which hinder the large-scale production in solar cells.[22,28] Commercial carbon paste exhibits excellent advantages of high conductivity, low cost, low-temperature process (100 °C), and good stability, which make it an excellent candidate for cathodes of perovskite-based solar cells.

Moreover, organometal halide perovskite has been considered as both light harvester and hole transporting material.[26−31] And the electron–hole diffusion length of $CH_3NH_3PbI_3$ can even exceed 100 nm.[32,33] All these evidences indicate that complicated hole–transport materials are not necessary in fabricating a simpler perovskite-based photovoltaic device.

In view of these reported results, herein, we report TiO_2/$CH_3NH_3PbI_3$/carbon structured heterojunction solar cells. Different from traditional perovskite solar cells, low-temperature-processed commercial carbon paste (100 °C) was developed as counter electrode to instead of Au or Ag. A

Received: June 27, 2014
Accepted: August 27, 2014
Published: August 27, 2014

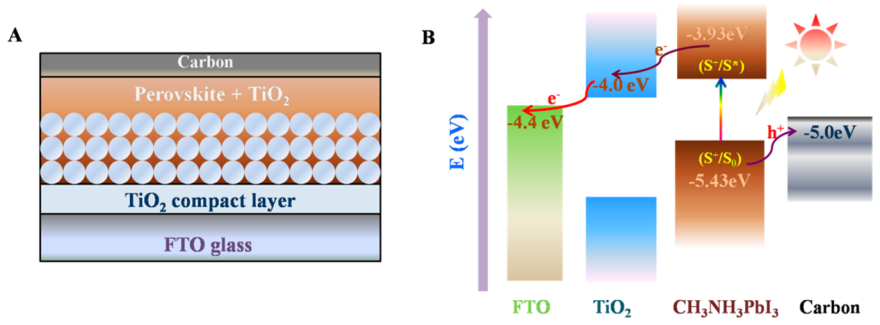

Figure 1. Device architeture and energy level diagram. (A) Device architecture of the cell tested in this study. (B) Energy levels (relative to vavuum) of various device components.

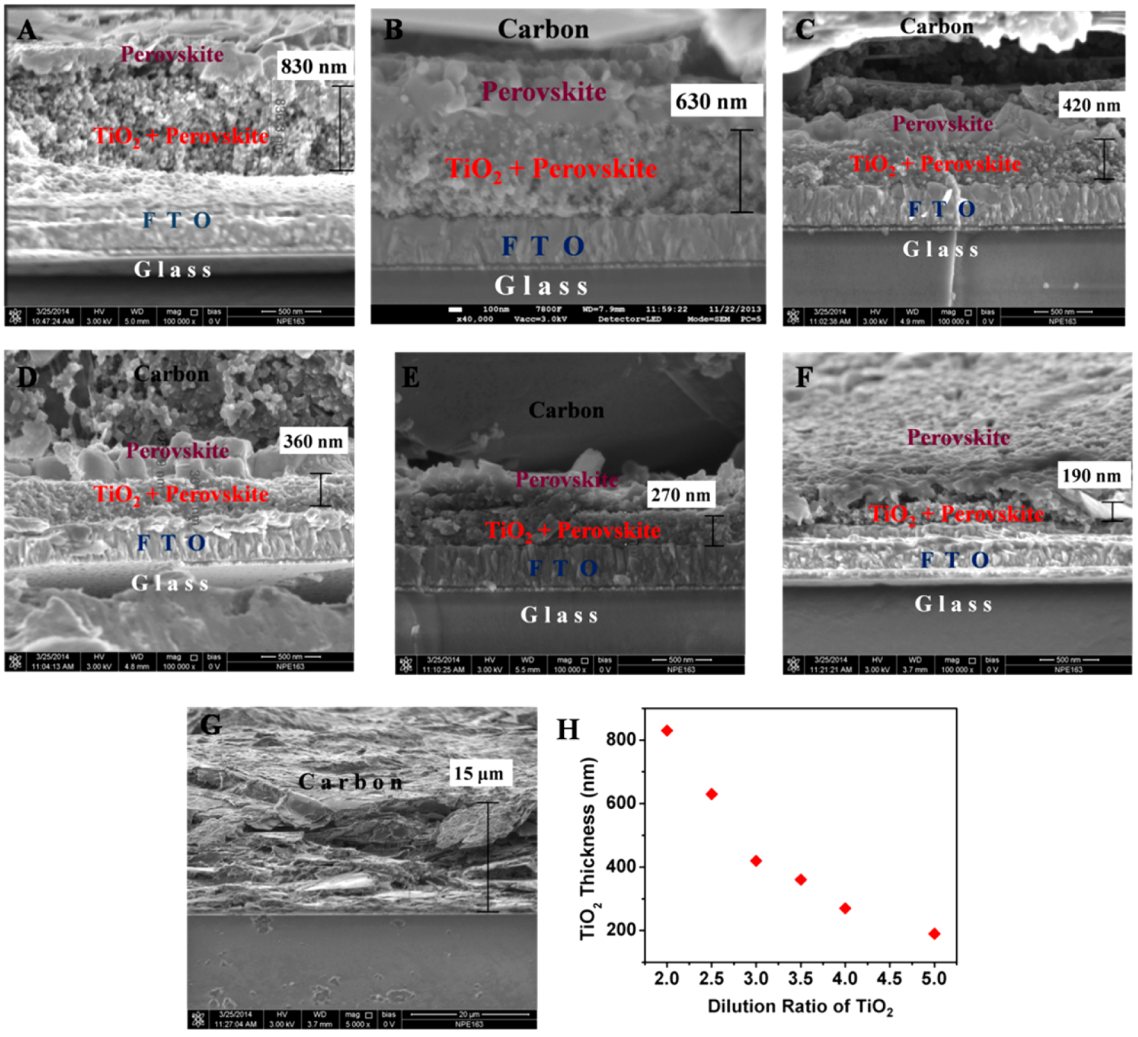

Figure 2. HR−SEM images of different TiO_2 film thickness-based devices. (A) Thickness of 830 nm TiO_2 film corresponds to dilution ratio of 1:2. (B) Thickness of 630 nm TiO_2 film corresponds to dilution ratio of 1:2.5. (C) Thickness of 420 nm TiO_2 film corresponds to dilution ratio of 1:3. (D) Thickness of 360 nm TiO_2 film corresponds to dilution ratio of 1:3.5. (E) Thickness of 270 nm TiO_2 film corresponds to dilution ratio of 1:4. (F) Thickness of 190 nm TiO_2 film corresponds to dilution ratio of 1:5. (G) Cross-section image of the whole device. (H) Relation schema of TiO_2 film thickness to dilution ratios.

remarkable photovoltaic performance with a short circuit (J_{SC}) of 16.78 mA/cm^2, an open circuit voltage (V_{OC}) of 0.90 V, and a fill factor (FF) of 55.0%, corresponding to a *PCE* of 8.31%, and high stability were achieved. The electrochemical impedance spectroscopy (EIS) measurements demonstrated that holes in perovskite could be transported effectively to carbon counter electrode. To the best of our knowledge, this is the first report for the use of low temperature processed carbon paste as counter electrode in hole−conductor free perovskite−based solar cells.

2. EXPERIMENTAL SECTION

Full details of the device fabrication and characterization are provided in the Supporting Information. Devices were fabricated on fluorine

doped tin oxide (FTO) coated glass serving as transparent electrode and substrate, respectively. A compact layer of TiO_2 was deposited by spin-coating from a precursor solution to act as an electron blocking layer to prevent shunting and leakage currents. Mesoporous TiO_2 (mp-TiO_2) film was deposited by spin-coating a diluted TiO_2 paste (18NR-T Dyesol), followed by sintering at 500 °C. Upon cooling to room temperature, the perovskite was deposited by spin-coating a γ-butyrolacetone solution of methylammonium iodide and PbI_2 (1:1 molar ratio), which formed the perovskite after heating at 100 °C for 15 min. Finally, devices were completed by depositing commercial carbon paste on the top of the perovskite film by the doctor-blading technique, followed by heat-treatment at 100 °C for 30 min. Devices were measured under simulated AM 1.5 G, 100 mW cm^{-2} sun light with an active area of 0.12 cm^2. All layers of the as-prepared devices are illustrated in Figure 1A.

3. RESULTS AND DISCUSSION

3.1. Optical and Electronic Properties. The energy levels of the materials used to prepare the solar cells are depicted in Figure 1B. The valence band (VB) and conduction band (CB) of the perovskite are −5.43 and −3.93 eV, versus vacuum, respectively.[29] Once illuminated by sunlight, the $CH_3NH_3PbI_3$ was excited from ground state to excited state, free charge carriers (or excitons, electron/hole pairs) generated in the $CH_3NH_3PbI_3$ layer can be dissociated at the interfaces of mesoporous TiO_2/$CH_3NH_3PbI_3$. The conduction and valence bands of the $CH_3NH_3PbI_3$ permit electron injection into TiO_2 (−4.0 eV), and the hole transport to the carbon cathode (−5.0 eV).[22]

The prepared $CH_3NH_3PbI_3$/mp-TiO_2/compact TiO_2/FTO film was further characterized by UV−Vis absorbance spectrum and X−ray diffraction (XRD) spectroscopy (see Figures S1 and S2 in the Supporting Information). The darkened film shows a wide absorption response from visible to near-infrared, which indicates the formation of $CH_3NH_3PbI_3$ in the solid state. The appearance of strong peaks at 2θ = 13.5, 28.35, 31.7, 40.45, and 43.14° in Figure S2 in the Supporting Information corresponding to the (110), (220), (310), (224,) and (314) planes, confirm the formation of tetragonal perovskite structure further.[34,35]

3.2. Photovoltaic Performance. The width of depletion region formed in this TiO_2/perovskite heterojunction is of great significance for the performance of this solar cell. With the same concentration of perovskite precursor, the depletion region width of this heterojunction solar cell was dominated by the thickness of TiO_2 films.[30,31,36] So the influence on the performance of the TiO_2 film thickness was investigated by diluting TiO_2 paste to various ratios and fabricating devices under the same experiment conditions in the same batch.

The relation schema of the film thickness and dilution ratios is shown in Figure 2H. Figure 2A−F presents cross-sectional high resolution scanning electron microscopy (HR−SEM) images of representative devices with various TiO_2 thickness. From the SEM images, we detected that different thickness of $CH_3NH_3PbI_3$ perovskite overlayers formed on top of TiO_2 films. and the perovskite penetrated into the mesoporous TiO_2 film in varying degrees, which is conducive to the formation of TiO_2/ $CH_3NH_3PbI_3$ heterojuction. The thickness of carbon counter electrode is about 15 μm as observed in Figure 2G.

The photocurrent density−voltage characteristics (*J*−*V*) curves of TiO_2/ $CH_3NH_3PbI_3$/carbon heterojunction solar cells fabricated with various TiO_2 film thicknesses are shown in Figure 3, and the corresponding characteristic parameters are summarized in Table 1. From this table, the highest efficiency

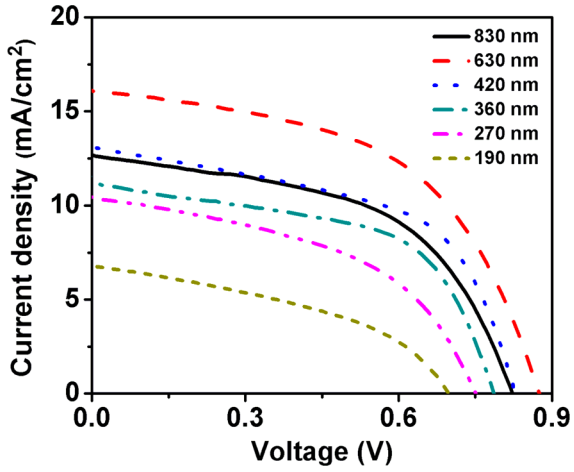

Figure 3. *J*−*V* curves of the perovskite-based heteojunction solar cell with different TiO_2 film thickness.

Table 1. Photovoltaic Performances of TiO_2/$CH_3NH_3PbI_3$/Carbon Heterojunction Solar Cell Obtained for Various TiO_2 Film Thickness in Same Batch

mp−TiO_2 thickness (nm)	830	630	420	360	270	190
J_{SC} (mA/cm^2)	12.67	16.10	13.41	11.43	10.43	6.94
V_{OC} (V)	0.82	0.87	0.83	0.78	0.75	0.70
FF (%)	52.60	52.60	54.28	55.08	47.72	41.09
PCE (%)	5.48	7.40	6.02	4.91	3.71	2.00

of 7.4% was observed for the solar cells made with mp-TiO_2 films of 630 nm thickness. Under different film thickness condition, efficiencies of 5.48, 7.40, 6.02, 4.91, 3.71, and 2.00% were achieved corresponding to film thickness of 830, 630, 420, 360, 270, and 190 nm separately. Disciplines between film thickness and device performance can be drawn from this set of data. As the film thickness decrease from 630 to 190 nm, the J_{SC} and V_{OC} of these cells decrease from 16.10 to 6.94 mA/cm^2 and from 870 to 700 mV, respectively. This phenomenon can be explained by that too thin TiO_2 film can not support enough thickness of perovskite, thereby yields a narrow depletion region, which cannot separate electron−hole pairs efficiently,[31] correspondingly result in an inferior V_{OC} and J_{SC}. With the increased thickness of mp-TiO_2 film (from 630 to 830 nm), the efficiency drops sharply to 5.48% (J_{SC} = 12.67 mA/cm^2, V_{OC} = 0.82 V, FF = 52.60%). This is mainly due to a thicker TiO_2 film leading to serious recombination of the injected electron in the TiO_2 CB with the hole in perovskite.

A champion PCE of 8.31% was achieved with the optimum TiO_2 film thickness of 630 nm after careful optimization. The current−voltage (*J*−*V*) characteristics and incident photon-to-current efficiency (IPCE) spectrum of the highest-performing device are shown in Figure 4. And the corresponding data are collected in Table 2. From the *J*−*V* curve measured under standard AM 1.5G illumination, the J_{SC}, V_{OC}, fill factor, and PCE were determined as 16.78 mA/cm^2, 0.90 V, 55%, and 8.31%, respectively.

Incident photon-to-electron conversion efficiency (IPCE) spectrum was employed to describe external quantum efficiency of extracted electrons from incident photons at different wavelengths, which is directly related to the J_{SC}. As displayed in Figure 4B, a wide response in the range of 400−800 nm can be observed for this $CH_3NH_3PbI_3$/TiO_2 heterojunction solar cell.

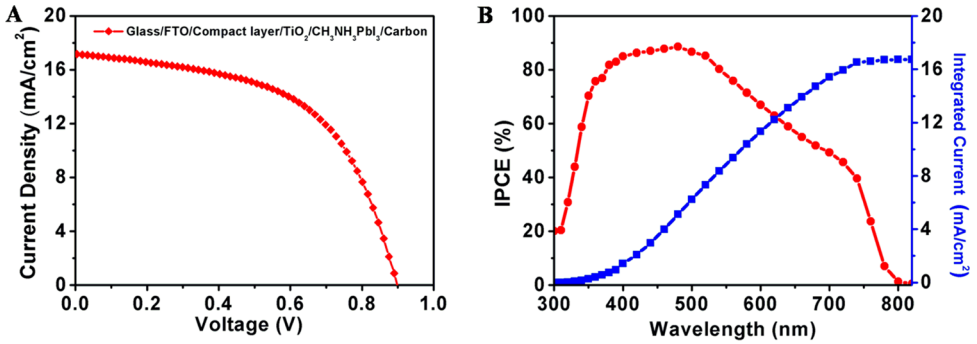

Figure 4. (A) Current density−voltage (J−V) curve and (B) IPCE spectrum of the optimized performing $CH_3NH_3PbI_3/TiO_2$ heterojunction solar cell.

Table 2. Photovoltaic Performance of the Optimum $CH_3NH_3PbI_3/TiO_2$ Heterojuction Solar Cell

photo sensitizer	J_{SC} (mA/cm^2)	V_{OC} (V)	FF (%)	PCE (%)
$CH_3NH_3PbI_3$	16.78	0.90	55.00	8.31

The onset of photocurrent at 800 nm is consistent with the band gap of the $CH_3NH_3PbI_3$.[8] Especially, the IPCE value exceeding 80% in range 400−540 nm was detected. Moreover, integrating the IPCE spectrum with the AM 1.5G solar photon flux yields a current density of 16.73 mA/cm^2, which is in good agreement with the test result displayed in Table 2.

3.3. Mott−Schottky Analysis. Several reports[30,31] have confirmed the existence of the depletion layer created in the $CH_3NH_3PbI_3$ perovskite film and in mp-TiO_2 film. This depletion layer assists in the charge separation and inhibits the back reaction of electrons from TiO_2 to $CH_3NH_3PbI_3$ film. The width of the depletion layer is of great importance for the performance of this heterojunction solar cell, in which the mobile charge carriers have been forced away by an electric field, the only elements left in the depletion region are ionized donor or acceptor impurities. To further understand the operation mechanism of the best-performed commercial carbon CE-based $TiO_2/CH_3NH_3PbI_3$ heterojunction solar cell, we carried out capacitance−voltage measurement (Mott−Schottky analysis[37]) to estimate the depletion region width and doping density of $CH_3NH_3PbI_3$ in this commercial carbon CE-based solar cell. The result is presented in Figure 5.

The capacitance of TiO_2/ $CH_3NH_3PbI_3$ heterojuncton is described in eq 1 calculated from the depletion approximation,[38] which implies that there are no free carriers in this depletion region at the junction under investigation.

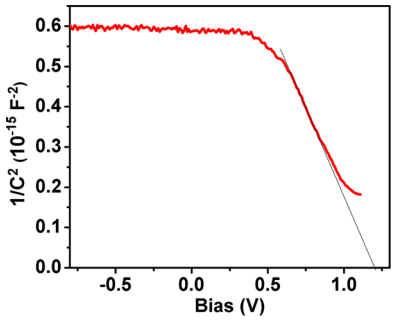

Figure 5. Mott−Schottky analysis at 1 kHz for the TiO_2/ $CH_3NH_3PbI_3$/carbon heterojunction solar cell.

$$\frac{1}{C^2} = \frac{2}{\varepsilon\varepsilon_0 q A^2 N}(V_{bi} - V) \quad (1)$$

Where C is the measured capacitance, A is the active area, V is the applied bias, V_{bi} is the built-in potential, ε is the static permittivity, ε_0 is the permittivity of free space, q is the elementary charge, and N is the doping density of the donor. According to previous researches, the static permittivity of $CH_3NH_3PbI_3$ was measured and calculated to be 30.[39] The slope of $1/C^2$ vs. V in the linear regime was 0.93×10^{15} F^{-2} V^{-1}, from which the net doping density in the $CH_3NH_3PbI_3$ film is found to be 3.51×10^{17} cm^{-3}. While the built−in potential can be calculated to be 1.2 V from the interception of the linear regime with the x-axis of the Mott−Schottky plot in Figure 5, which can suppress the back reaction of electrons from the TiO_2 film to $CH_3NH_3PbI_3$ film efficiently.

The depletion width is calculated according to eq 2[40]

$$W_{p,n} = \frac{1}{N_{a,d}}\sqrt{\frac{2\varepsilon V_{bi}}{q\left(\frac{1}{N_a + N_d}\right)}} \quad (2)$$

Where N_a and N_d are the doping densities of the acceptor and donor, respectively. The mp-TiO_2 doping density starts at $N_a = 1 \times 10^{16}$ cm^{-3}.[41,42] According to this equation, the depletion width on the TiO_2 side was calculated to be 281 nm and on the $CH_3NH_3PbI_3$ side 78 nm, respectively. A 630 nm thick mp-TiO_2 and 400 nm thick $CH_3NH_3PbI_3$ overlayer can be observed in the case of the optimized efficiency device in Figure 2B. This suggests that almost half of the TiO_2 film is depleted (depleted fraction equals to 0.45), whereas more than a fifth of the perovskite layer have been depleted, which is consistent with the Etgar's work.[31] Moreover, the photogenerated carrier could be separated more efficiently in such a wide built-in field of the depletion region, which contributes to higher power conversion efficiency of the cell.

3.4. Electrochemical Impedance Spectroscopy Analysis. To further evaluate the influence of the low-temperature processed commercial carbon counter electrode on the performance of solar cells, we carried out EIS measurements in the frequency range 100 mHz to 1 MHz with 10 mV AC amplitude under one sun illumination (Figure 6A) and in dark (Figure 6B) conditions. And the equivalent circuit is present in the inset in Figure 6A. Figure 6 depicts the Nyquist plots of solar cells fabricated with commercial carbon CEs at a bias of −0.8 V. The RC response in the high-frequency region is assigned to the charge exchange process at the $CH_3NH_3PbI_3$/ carbon CE interface, whereas the one at the low-frequency

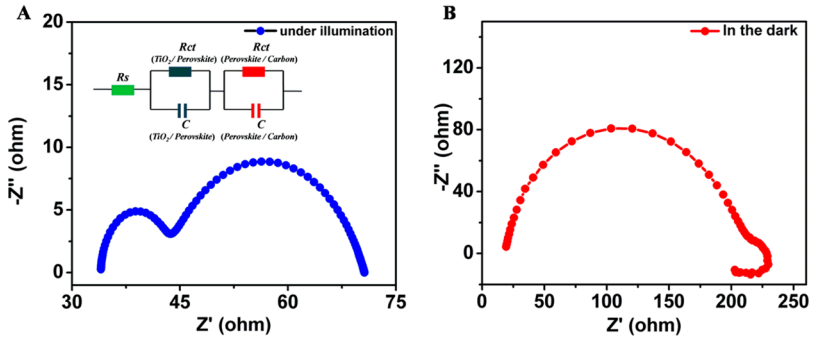

Figure 6. Nyquist plots of commercial carbon CE-based solar cells (A) under illumination and (B) in dark condition. Inset: the equivalent circuit employed to fit the spectra.

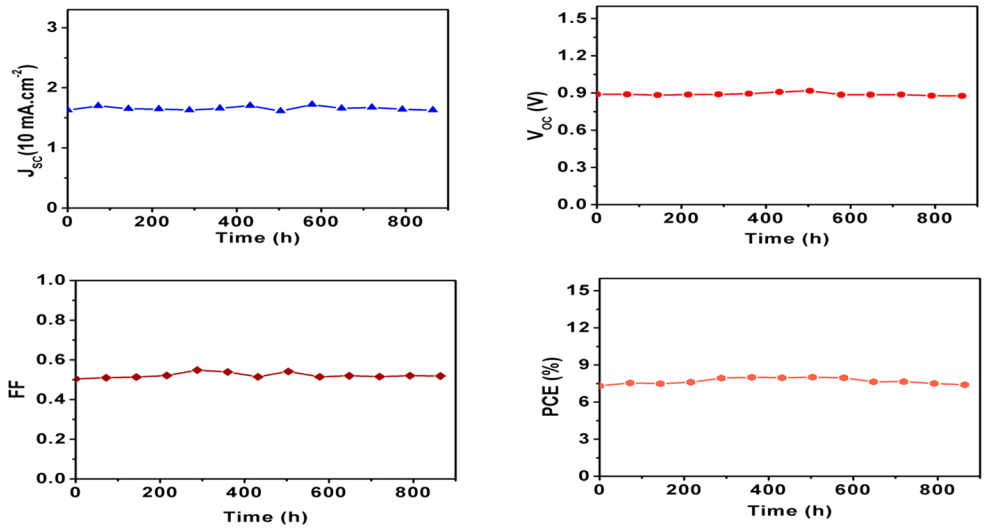

Figure 7. Long-term stability of the cell stored in ambient atmosphere at room temperature without encapsulation and measured under one sun illumination.

region represents the $TiO_2/CH_3NH_3PbI_3$ interface. When it was illuminated under one sun light, two semicircles can be found in the Nyquist plot. And a low R_{CT} of 8.9 ohm was detected at the interface of $CH_3NH_3PbI_3$/carbon CE in the high-frequency region. In the dark condition, there are two RC elements and a negative capacitance can be discovered in Nyquist plot, in which the large arc in the high-frequency region is ascribed to the charge transport impedance at the interface of $CH_3NH_3PbI_3$/carbon and the negative capacitance appears in the low frequencies is assigned to a additional recombination pathway at high bias at one of the interface. A smaller radius of semicircle compared than previous report is also detected in Nyquist plot derived from dark condition.[43] The low R_{CT} found in dark and illuminating condition contribute to better transport of holes from perovskite to carbon CEs, which indicates that the low-temperature-processed carbon can work well when worked as counter electrode for perovskite solar cell.

3.5. Stability Analysis. Finally, the stability of this commercial carbon-paste-based $CH_3NH_3PbI_3/TiO_2$ heterojunction solar cell stored in ambient atmosphere at room temperature without encapsulation was tested and the detailed photovoltaic parameters were plotted in Figure 7. As is known to all of us, the stability of perovskite solar devices is limited mainly to the ambient moisture because the alkylammonium salts are, in general, highly hygroscopic.[44] However, the photovoltaic performances of representative perovskite solar cells demonstrate high stability in this carbon-based devices. To be specific, during the tests, the PCE shifted from the initial 7.31% to the final 7.42%, and an average PCE of 7.57% was achieved. Furthermore, an average J_{SC} 16.65 mA/cm^2, V_{OC} 0.89 V, and FF 53.0% were achieved over the 800 h test. This remarkable stability should be attributed to the thick carbon cathode layer, which can work as a water-retaining layer to protect the perovskite from being destroyed.[45] This result indicates the underlying potential of commercial carbon paste as promising candidates for highly efficient perovskite solar cell.

4. CONCLUSION

In summary, low-temperature-processed (100 °C) carbon paste was developed as counter electrode material in hole−transport materials free perovskite/TiO_2 heterojunction solar cells to substitute noble metallic materials. Through detailed studies we found that the thickness of mp-TiO_2 film has great effects on photovoltaic performance of solar cells. Under optimized conditions, an impressive PCE value of 8.31% has been achieved with this carbon counter electrode. Impedance spectroscopy demonstrates good charge transport characteristics of low-temperature-processed carbon counter electrode. Moreover, long-term stability investigations show that this carbon counter electrode-based perovskite solar cells exhibit good stability over 800 h. This structured solar cell simplifies

production procedure and facilitates commercial production. These exciting results demonstrate that cost-effective and better performance for Perovskite-based solar cell can indeed be achieved in future commercialization. And we fully believe that there is still great room for fabricating higher-performance solar cells using this carbon counter electrode.

■ ASSOCIATED CONTENT

Supporting Information

Detailed device fabricating procedures, characterizations of the solar cells, UV−Vis absorbance spectrum, X−ray diffraction (XRD) spectroscopy, the performance comparison with gold counter electrode, as well as photovoltaic parameters of 20 devices. This material is available free of charge via the Internet at http://pubs.acs.org/.

■ AUTHOR INFORMATION

Corresponding Author

*E-mail: yangxc@dlut.edu.cn.

Notes

The authors declare no competing financial interest.

■ ACKNOWLEDGMENTS

We gratefully acknowledge the financial support of this work from China Natural Science Foundation (Grant 21276044, 21120102036, 91233201) and the National Basic Research Program of China (Grant 2014CB239402).

■ REFERENCES

(1) Sargent, E. H. Colloidal Quantum Dot Solar Cells. *Nat. Photonics* **2012**, *6*, 133−135.

(2) Liu, Y.; Chen, C.-C.; Hong, Z.; Gao, J.; Yang, Y.; Zhou, H.; Dou, L.; Li, G.; Yang, Y., Solution-Processed Small-Molecule Solar Cells: Breaking the 10% Power Conversion Efficiency. *Sci. Rep.* **2013**, *3*.

(3) Burschka, J.; Dualeh, A.; Kessler, F.; Baranoff, E.; Cevey-Ha, N. L.; Yi, C.; Nazeeruddin, M. K.; Gratzel, M. Tris(2-(1H-pyrazol-1-yl)pyridine)cobalt(III) as P-type Dopant for Organic Semiconductors and Its Application in Highly Efficient Solid-state Dye-Sensitized Solar Cells. *J. Am. Chem. Soc.* **2011**, *133*, 18042−18045.

(4) Ip, A. H.; Thon, S. M.; Hoogland, S.; Voznyy, O.; Zhitomirsky, D.; Debnath, R.; Levina, L.; Rollny, L. R.; Carey, G. H.; Fischer, A.; Kemp, K. W.; Kramer, I. J.; Ning, Z.; Labelle, A. J.; Chou, K. W.; Amassian, A.; Sargent, E. H. Hybrid Passivated Colloidal Quantum Dot Solids. *Nat. Nanotechnol.* **2012**, *7*, 577−582.

(5) Kim, H.-S.; Lee, C.-R.; Im, J.-H.; Lee, K.-B.; Moehl, T.; Marchioro, A.; Moon, S.-J.; Humphry-Baker, R.; Yum, J.-H.; Moser, J. E.; Gratzel, M.; Park, N.-G., Lead Iodide Perovskite Sensitized All-Solid-State Submicron Thin Film Mesoscopic Solar Cell with Efficiency Exceeding 9%. *Sci. Rep.* **2012**, *2*.

(6) Lee, M. M.; Teuscher, J.; Miyasaka, T.; Murakami, T. N.; Snaith, H. J. Efficient Hybrid Solar Cells Based on Meso-Superstructured Organometal Halide Perovskites. *Science.* **2012**, *338*, 643−647.

(7) Wehrenfennig, C.; Eperon, G. E.; Johnston, M. B.; Snaith, H. J.; Herz, L. M. High Charge Carrier Mobilities and Lifetimes in Organolead Trihalide Perovskites. *Adv. Mater.* **2014**, *26*, 1584−1589.

(8) Papavassiliou, G. C. Synthetic Three-and Lower-Dimensional Semiconductors Based on Inorganic Units. *Mol. Cryst. Liq. Cryst. Sci. Technol., Sect. A* **1996**, *286*, 231−238.

(9) Stoumpos, C. C.; Malliakas, C. D.; Kanatzidis, M. G. Semiconducting Tin and Lead Iodide Perovskites with Organic Cations: Phase Transitions, High Mobilities, and Near-Infrared Photoluminescent Properties. *Inorg. Chem.* **2013**, *52*, 9019−9038.

(10) Ball, J. M.; Lee, M. M.; Hey, A.; Snaith, H. J. Low-Temperature Processed Meso-Superstructured to Thin-Film Perovskite Solar Cells. *Energy Environ. Sci.* **2013**, *6*, 1739−1743.

(11) Chen, Q.; Zhou, H.; Hong, Z.; Luo, S.; Duan, H.-S.; Wang, H.-H.; Liu, Y.; Li, G.; Yang, Y. Planar Heterojunction Perovskite Solar Cells via Vapor-Assisted Solution Process. *J. Am. Chem. Soc.* **2013**, *136*, 622−625.

(12) Heo, J. H.; Im, S. H.; Noh, J. H.; Mandal, T. N.; Lim, C.-S.; Chang, J. A.; Lee, Y. H.; Kim, H.-j.; Sarkar, A.; NazeeruddinMd, K.; Gratzel, M.; Seok, S. I. Efficient Inorganic-Organic Hybrid Heterojunction Solar Cells Containing Perovskite Compound and Polymeric Hole Conductors. *Nat. Photonics* **2013**, *7*, 486−491.

(13) Liu, D.; Kelly, T. L. Perovskite Solar Cells with a Planar Heterojunction Structure Prepared Using Room-Temperature Solution Processing Techniques. *Nat. Photonics* **2013**, *8*, 133.

(14) Liu, M.; Johnston, M. B.; Snaith, H. J. Efficient Planar Heterojunction Perovskite Solar Cells by Vapour Deposition. *Nature.* **2013**, *501*, 395−398.

(15) Malinkiewicz, O.; Yella, A.; Lee, Y. H.; Espallargas, G. M.; Graetzel, M.; Nazeeruddin, M. K.; Bolink, H. J. Perovskite Solar Cells Employing Organic Charge-Transport Layers. *Nat. Photonics* **2013**, *8*, 128−132.

(16) Burschka, J.; Pellet, N.; Moon, S. J.; Humphry-Baker, R.; Gao, P.; Nazeeruddin, M. K.; Gratzel, M. Sequential Deposition As a Route to High-Performance Perovskite-Sensitized Solar Cells. *Nature.* **2013**, *499*, 316−319.

(17) Wang, J. T.-W.; Ball, J. M.; Barea, E. M.; Abate, A.; Alexander-Webber, J. A.; Huang, J.; Saliba, M.; Mora-Sero, I.; Bisquert, J.; Snaith, H. J.; Nicholas, R. J. Low-Temperature Processed Electron Collection Layers of Graphene/TiO_2 Nanocomposites in Thin Film Perovskite Solar Cells. *Nano Lett.* **2013**, *14*, 724−730.

(18) Noh, J. H.; Im, S. H.; Heo, J. H.; Mandal, T. N.; Seok, S. I. Chemical Management for Colorful, Efficient, and Stable Inorganic-Organic Hybrid Nanostructured Solar Cells. *Nano Lett.* **2013**, *13*, 1764−1769.

(19) Wojciechowski, K.; Saliba, M.; Leijtens, T.; Abate, A.; Snaith, H. J. Sub-150 [degree]C Processed Meso-Superstructured Perovskite Solar Cells with Enhanced Efficiency. *Energy Environ. Sci.* **2014**, *7*, 1142−1147.

(20) Jeon, N. J.; Lee, H. G.; Kim, Y. C.; Seo, J.; Noh, J. H.; Lee, J.; Seok, S. I. o-Methoxy Substituents in Spiro-OMeTAD for Efficient Inorganic−Organic Hybrid Perovskite Solar Cells. *J. Am. Chem. Soc.* **2014**, *136*, 7837−7840.

(21) Zhou, H.; Chen, Q.; Li, G.; Luo, S.; Song, T.-b.; Duan, H.-S.; Hong, Z.; You, J.; Liu, Y.; Yang, Y. Interface Engineering of Highly Efficient Perovskite Solar Cells. *Science* **2014**, *345* (6196), 542−546.

(22) Ku, Z.; Rong, Y.; Xu, M.; Liu, T.; Han, H. Full Printable Processed Mesoscopic $CH_3NH_3PbI_3/TiO_2$ Heterojunction Solar Cells with Carbon Counter Electrode. *Sci. Rep.* **2013**, *3*, 3132.

(23) Dillon, A. C. Carbon Nanotubes for Photoconversion and Electrical Energy Storage. *Chem. Rev.* **2010**, *110*, 6856−6872.

(24) Zhang, Q.; Uchaker, E.; Candelaria, S. L.; Cao, G. Nanomaterials for Energy Conversion and Storage. *Chem. Soc. Rev.* **2013**, *42*, 3127−3171.

(25) Wu, M.; Lin, X.; Wang, T.; Qiu, J.; Ma, T. Low-Cost Dye-Sensitized Solar Cell Based on Nine Kinds of Carbon Counter ELectrodes. *Energy Environ. Sci.* **2011**, *4*, 2308−2315.

(26) Shi, J.; Dong, J.; Lv, S.; Xu, Y.; Zhu, L.; Xiao, J.; Xu, X.; Wu, H.; Li, D.; Luo, Y.; Meng, Q. Hole-Conductor-Free Perovskite Organic Lead Iodide Heterojunction Thin-Film Solar Cells: High Efficiency and Junction Property. *Appl. Phys. Lett.* **2014**, *104*, 063901.

(27) Shi, J.; Luo, Y.; Wei, H.; Luo, J.; Dong, J.; Lv, S.; Xiao, J.; Xu, Y.; Zhu, L.; Xu, X.; Wu, H.; Li, D.; Meng, Q. Modified Two-Step Deposition Method for High-Efficiency $TiO_2/CH_3NH_3PbI_3$ Heterojunction Solar Cells. *ACS Appl. Mater. Interfaces* **2014**, *6*, 9711−9718.

(28) Rong, Y.; Ku, Z.; Mei, A.; Liu, T.; Xu, M.; Ko, S.; Li, X.; Han, H. Hole-Conductor-Free Mesoscopic $TiO_2/CH_3NH_3PbI_3$ Heterojunction Solar Cells Based on Anatase Nanosheets and Carbon Counter Electrodes. *J. Phys. Chem. Lett.* **2014**, *5*, 2160−2164.

(29) Etgar, L.; Gao, P.; Xue, Z.; Peng, Q.; Chandiran, A. K.; Liu, B.; Nazeeruddin, M. K.; Grätzel, M. Mesoscopic $CH_3NH_3PbI_3/TiO_2$

Heterojunction Solar Cells. *J. Am. Chem. Soc.* **2012**, *134*, 17396−17399.
(30) Laban, W. A.; Etgar, L. Depleted Hole Conductor-Free Lead Halide Iodide Heterojunction Solar Cells. *Energy Environ. Sci.* **2013**, *6*, 3249−3253.
(31) Aharon, S.; Gamliel, S.; Cohen, B. E.; Etgar, L. Depletion Region Effect of Highly Eficient Hole Conductor Free $CH_3NH_3PbI_3$ Perovskite Solar Cells. *Phys. Chem. Chem. Phys.* **2014**, *16*, 10512−10518.
(32) Stranks, S. D.; Eperon, G. E.; Grancini, G.; Menelaou, C.; Alcocer, M. J.; Leijtens, T.; Herz, L. M.; Petrozza, A.; Snaith, H. J. Electron-Hole Diffusion Lengths Exceeding 1 Micrometer in an Organometal Trihalide Perovskite Absorber. *Science* **2013**, *342*, 341−344.
(33) Xing, G.; Mathews, N.; Sun, S.; Lim, S. S.; Lam, Y. M.; Gratzel, M.; Mhaisalkar, S.; Sum, T. C. Long-Range Balanced Electron- and Hole-Transport Lengths in Organic-Inorganic $CH_3NH_3PbI_3$. *Science* **2013**, *342*, 344−347.
(34) Im, J. H.; Lee, C. R.; Lee, J. W.; Park, S. W.; Park, N. G. 6.5% Efficient Perovskite Quantum-Dot-Sensitized Solar Cell. *Nanoscale* **2011**, *3*, 4088−4093.
(35) Kojima, A.; Teshima, K.; Shirai, Y.; Miyasaka, T. Organometal Halide Perovskites as Visible-Light Sensitizers for Photovoltaic. *J. Am. Chem. Soc.* **2009**, *17*, 6050−6051.
(36) Masahito, Z.; Atsushi, S.; Tsuyoshi, A.; Takeo, O. Fabrication and Characterization of $TiO_2/CH_3NH_3PbI_3$-based Photovoltaic Devices. *Chem. Lett.* **2014**, *43*, 916−918.
(37) Schottky, W. Vereinfachte und erweiterte Theorie der Randschicht-gleichrichter. *Z. Phys.* **1942**, *118*, 539−592.
(38) Clifford, J. P.; Johnston, K. W.; Levina, L.; Sargent, E. H. Schottky Barriers to Colloidal Quantum Dot Films. *Appl. Phys. Lett.* **2007**, *91*, 253117.
(39) Poglitsch, A.; Weber, D. Dynamic Disorder in Methylammonium Trihalogen Oplumbates (II) Observed by Millimeter-Wave Spectroscopy. *J. Chem. Phys.* **1987**, *8*, 6373−6378.
(40) Luther, J. M.; Law, M.; Beard, M. C.; Song, Q.; Reese, M. O.; Ellingson, R. J.; Nozik, A. J. Schottky Solar Cells Based on Colloidal Nanocrystal Films. *Nano. lett.* **2008**, *8*, 3488−3492.
(41) Nakade, S.; Saito, Y.; Kubo, W.; Kanzaki, T.; Kitamura, T.; Wada, Y.; Yanagida, S. Enhancement of Electron Transport in Nano-Porous TiO_2 Electrodes by Dye Adsorption. *Electrochem. Commun.* **2003**, *5*, 804−808.
(42) Zaban, A.; Meier, A.; Gregg, B. A. Electric Potential Distribution and Short-Range Screening in Nanoporous TiO_2 Electrodes. *J. Phys. Chem. B* **1997**, *101*, 7985−7990.
(43) Xu, M.; Rong, Y.; Ku, Z.; Mei, A.; Liu, T.; Zhang, L.; Li, X.; Han, H. Highly Ordered Mesoporous Carbon for Mesoscopic $CH_3NH_3PbI_3/TiO_2$ Heterojunction Solar Cell. *J. Mater. Chem. A* **2014**, *2*, 8607−8611.
(44) Suarez, B.; Gonzalez-Pedro, V.; Ripolles, T. S.; Sanchez, R. S.; Otero, L.; Mora-Sero, I. Recombination Study of Combined Halides (Cl, Br, I) Perovskite Solar Cells. *J. Phys. Chem. Lett.* **2014**, *5*, 1628−1635.
(45) Mei, A.; Li, X.; Liu, L.; Ku, Z.; Liu, T.; Rong, Y.; Xu, M.; Hu, M.; Chen, J.; Yang, Y.; Grätzel, M.; Han, H. A Hole-Conductor-Free, Fully Printable Mesoscopic Perovskite Solar Cell with High Stability. *Science* **2014**, *345*, 295−298.